

# A Multiple Neural Network System to Classify Solder Joints on Integrated Circuits

G. Acciani, G. Brunetti and G. Fornarelli

Politecnico di Bari, Dipartimento di Elettrotecnica ed Elettronica,  
Via E. Orabona 4, Bari 70125, Italia  
[acciani@poliba.it](mailto:acciani@poliba.it), [lab.pin@deemail.poliba.it](mailto:lab.pin@deemail.poliba.it), [fornarelli@deemail.poliba.it](mailto:fornarelli@deemail.poliba.it)

**Abstract:** The following paper introduces a diagnostic process to detect solder joint defects on Printed Circuit Boards assembled in Surface Mounting Technology. The diagnosis is accomplished by a Neural Network System which processes the images of the solder joints of the integrated circuits mounted on the board. The board images are acquired and then pre-processed to extract the regions of interest for the diagnosis which are the solder joints of the integrated circuits. Five different levels of solder quality in respect to the amount of solder paste have been defined. Two feature vectors have been extracted from each region of interest, the “geometric” feature vector and the “wavelet” feature vector. Both vectors feed the neural network system constituted by two Multi Layer Perceptron neural networks and a Linear Vector Quantization network for the classification. The experimental results are devoted to comparing the performances of a Multi Layer Perceptron network, of a Linear Vector Quantization network, and of the overall neural network system, considering both geometric and wavelet features. The results prove that the overall classifier is the best compromise in terms of recognition rate and time required for the diagnosis in respect to the single classifiers.

**Keywords:** PCB, SMT, feature extraction, Wavelet transform, Multiple Neural Network System.

## I. Introduction

One of the most common technologies used in producing Printed Circuit Boards (PCBs) is the Surface Mounted Technology (SMT). By employing SMT, the production process speeds up but the risk of defects increases because of the miniaturization of the components, the denser packing of boards and the highly automated assembly equipment. In these conditions the task of detecting defects becomes more critical and difficult.

The SMT production process consists of three main steps: 1) solder printing, where a solder paste layer is printed on the surface of the board; 2) pick and place, where each component is positioned on the board; 3) reflow where the solder joints take shape by the reflowing of the solder paste [1].

Solder Printing	Pick and Place	Reflow
Paste missing	Missing parts	Solder bridges
Misplaced paste print	Misoriented parts	Faulty solder joints
Smudged print	Damaged parts	Lifted leads
Paste bridges	Wrong parts	Raised parts
No wetting	Doubled parts	Tombstoned parts
Contamination	Face down	Solder balls

Table 1. Defects after each step of the production process.

Table 1 shows several defects that could occur during each step of the production process. These defects are commonly detected employing the in-circuit test (ICT), the functional test (FBT), the automated or manual visual inspection (MVI) or other means. However, PCB manufacturers find it difficult to gain physical test-probe access to dense, fine-pitch boards using the bed-of-nails test fixtures. Moreover, writing functional test programs is too expensive and time consuming for complex boards.

To overcome these difficulties, Automatic Optical Inspection (AOI) proves to be a useful supplement to ICT as well as to the functional test. Human inspectors still perform most inspections, but the progressive reduction of the board sizes have made manual inspection unreliable. In fact human inspection has a low repeatability level and visual fatigue inevitably leads to missed defects. For these reasons, AOI is gradually replacing human inspection on the assembly line. AOI typically uses visible light and cameras to acquire the images of the PCB and employs algorithms to verify that the product has been correctly assembled. With this technology the AOI is employed in several critical points of the production process in order to inspect the paste printing, the pre-reflow and the post-reflow component placement, as well as the correct forming of the solder joints.

Another contribution provided by an in-line AOI system is the capability to record all the results and compare them with all the other process parameters. These advantages and the simple technology described make AOI for PCB one of

the principal industrial applications for computerized image-analysis techniques.

In [2] Krippner and Beer show that the paste faults amount to only 8.3% of the whole printed circuit assembly process, while 90% percent of the faults, which consist of component and soldering faults, were detectable only after soldering. Moreover, 80% of the optically recognizable faults could not be recognized electrically. This result proves that optical inspection is necessary. It has been shown that paste inspection and component inspection detected a relatively high percentage of process faults which amounts to over 50%; however, they corrected themselves during the subsequent process steps. Paste or pre-reflow quality control is certainly a practical way to optimize the process avoiding mass production faults or recognizing faults in the production equipment, but a premature diagnosis would be inefficient and too costly. Though these results cannot be generalized, they show that post-reflow AOI is a key factor in the production process and is very well suited for detecting relevant faults.

Among the defects that could arise in the reflow step, faulty solder joints are extremely important. They could cause solder bridges and missing contacts that compromise the correct functioning of a PCB. For this reason, many works and various techniques have been developed to recognize faulty solder joints. In [3] Kim *et al.* develop a two-stage classifier to recognize four types of solder joints: good, none, insufficient and excess. They use three layers of ring-shaped LEDs to extract shape information of the solder joint. From this information they extract 2D features i.e. average grey level and highlight percentage to feed the first stage of the classifier, which is a Multi Layer Perceptron (MLP) network. In cases which are uncertain, they evaluate also 3D features to feed the second stage of the classifier which is a Bayes classifier. A three colour circular illumination system has been used also by Ko and Cho in [4], and by Yun *et al.* in [5].

A two-stage classifier has also been developed by S. Jagannathan to recognize three types of solder joints. In his work [6] Jagannathan employs the adaptative learning capabilities of a neural network to study the characteristics of the grey-level histogram of a solder joint image, so that some features can be extracted. These features are presented to a second stage of the neural network which selects and interprets them to produce the diagnosis.

A neural network approach has been developed also by Fanni *et al.* in [7] to classify three types of solder joints. They employ the Fast Fourier Transform (FFT) and the Haar Transform (HT) to extract two kinds of features from PCB images that feed an MLP classifier. By comparing the results of the solder joint tests, they prove that the HT has a better recognition rate.

Other authors have acquired X-ray images of PCB. Voci *et al.* [8] have developed a fuzzy rule based system for

recognizing short circuits developed during soldering process. Neubauer and Hanke [9] have integrated two MLP networks to detect solder pads. The first network decides from a low resolution image where the solder joint is located, the second network performs the diagnosis detecting the presence of voids within solder joints. Ko *et al.* [10] have developed a diagnosis system, constituted by an MLP and four Linear Vector Quantization (LVQ) neural networks to recognize three types of solder joints in a ball grid array. The LVQ networks are used to cluster the input of the grey level profiles of the image evaluated in four directions. The MLP network performs the diagnosis; its inputs are the Euclidean distances between the grey level profiles of the image in each direction and the weight vectors, that are the outputs of the LVQ networks.

Some of the methods described above have complex systems of image acquisition that need special illumination systems. Solder joint inspection is arguably the most difficult task for algorithm-based AOI systems because of the wide ranges in which the image parameters could vary. In addition, the proposed algorithms and the classification methods are generally able to recognize three or four types of solder joints and to improve their recognition rate it is often necessary to extract complex features, whose evaluation involves the knowledge of some of the physical parameters of the soldering process and of the high computational time.

One important stage of the diagnosis approach is to select the right method for the classification. This stage is not easy because there is a considerable overlap between the fields of different approaches and each method presents advantages and disadvantages. Often, given a specific problem, the choice of one approach instead of another can be made on the basis of analysis of underlying statistical components and perhaps through lack of suitable statistical or structural models [11]. This is an important criterion to select a classifier, in fact, in most applications it can not be assumed that the forms of the underlying density functions are known therefore the common parametric forms rarely fit the densities actually encountered in practice. For this reason the nonparametric procedures are the most suitable methods that can be used with arbitrary distributions and without the assumption that the forms of the underlying densities are known [12]. However, parametric statistical classification methods suffer from strong assumptions about the database, while nonparametric ones are unsuitable for small data sets. Neural network models do not require the same restrictive assumptions about the relationship between the independent variables and dependent variables as parametric statistical methods and can learn to generalize from noisy data. Therefore the neural networks represent an important and effective class of classifiers that satisfy the request for deeming the structure of the data sets and can successfully be used for the classification of anomaly detection in image processing. Moreover when multiple neural networks are used in the ensemble approach each network is trained using

the same inputs so that each network provides a solution for the same task. Outputs from these redundant networks are combined to reach an integrated result, mitigate the limitations of each constituent network and minimize the errors [13].

In this paper a multiple neural network based AOI system for solder joints inspection is presented. The proposed approach does not need a special illumination system or an advanced X-Y positioning system and the images of the board are acquired by an ordinary camera. Moreover, the evaluation of the features that feed the classification system do not require the knowledge of the physical parameter industrial process. Finally, the architecture of the neural network classifier allows a low computational time for the diagnosis.

The diagnostic process consists of three steps: 1) a pre-processing step in which the region of interest (ROI) for the diagnosis is extracted from the acquired image; 2) a feature extraction step in which the geometric features and the wavelet features are extracted from each ROI (solder joint); 3) a classification step in which a neural network system performs the diagnosis. This system can be included in the class of Multiple Neural Network Systems (MNNS) because it consists of two learning levels, the first formed by an MLP and an LVQ neural network, the second formed only by an MLP neural network. The inputs of the first level networks are geometric features of the image under test, while those of the second level are vectors which contain the above geometric features together with new features extracted by the wavelet transform. The second classification level analyzes only the images that are classified differently by the first level networks. In fact, in this case it may be supposed that one of them has performed a wrong classification so a new more accurate classification is necessary.

Five classes of solder joints in respect to the amount of solder paste have been analyzed.

The experimental results show that the MNNS performs the best compromise in recognition rate and time required for the diagnosis: the recognition rate is better than the single MLP and LVQ networks fed with both geometric and wavelet features, while the time required for the diagnosis is close to the lowest time taken by the single MLP and LVQ networks.

The paper is organized as follows: section II describes the overall diagnosis approach which consists of the pre-processing stage, the feature extraction stage and the classification stage; section III shows the results obtained by applying the proposed method to a database of PCB images. In conclusion the findings are summarized.

## II. Diagnosis approach

The acquiring system is constituted by a digital camera mounted on a X-Y positioning system that acquires the image of the PCB under test and by a personal computer

(Pentium 4 under Windows XP) that does the image processing and the final diagnosis.

The inspection procedure is summarized in the chart of figure 1. The first step is the board image acquisition. The image acquired by the camera (figure 2) contains the region of interest and also useless zones for the diagnosis. In the second step the ROI is extracted from an acquired image.

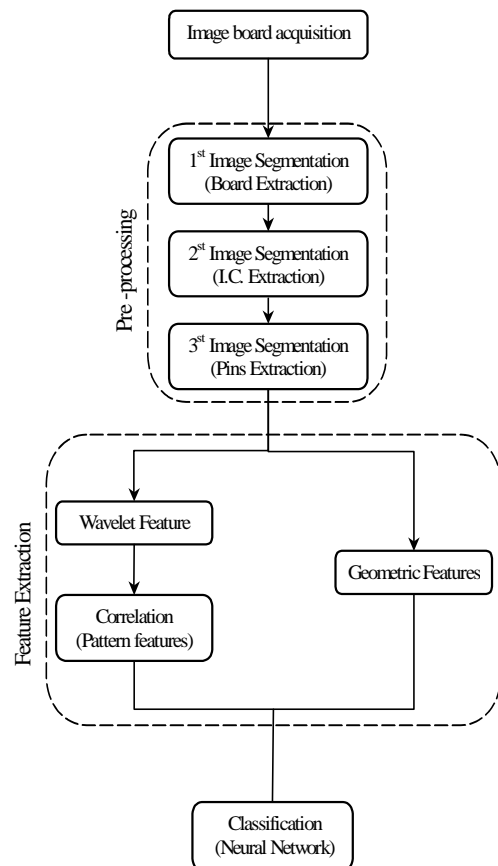
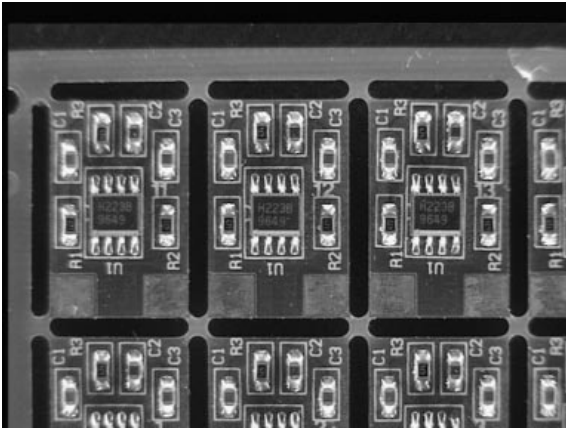


Figure 1. Inspection procedure

The ROI is represented by each pin of the integrated circuit mounted on each board. The third step of the diagnosis process is the feature extraction. In this step two kinds of features are extracted from each pin image: the geometric and the wavelet features. Finally, these features feed the network classifiers. Each of these steps is described in detail in the following subsection.

### A. Pre-processing

The acquired image shows more than one board but only the solder joints of the central one are under test. The task of the pre-processing stage is to obtain the ROI from the acquired images; this is achieved by three subsequent image segmentations. The first image segmentation extracts the board under inspection from the acquired image. Figure 3 shows the image after the first segmentation. In the second



**Figure 2.** Acquired image

step the image of the IC is extracted; this is shown in figure 4. The third image segmentation extracts the images of each solder joint (figure 5). The images shown in figure 3,4 and 5 have been obtained from the image of figure 2 by means of the three segmentations previously described.

It is important to highlight that the sequence of the three image segmentations described above allows the employment of an AOI system without an advanced positioning system and a digital camera for a direct acquisition of the pin image. Moreover, the solder images for each IC are obtained with short computational time in relation to the whole diagnosis time. The time taken for each step of the proposed approach will be given further on.

To perform the first image segmentation the features of the acquired images are matched with those of a reference image. The reference image is an image of the board as the one displayed in figure 4. The features are the "horizontal energy" and the "vertical energy" vectors of the image turned into grey scale.

Let  $I$  denote a  $p \times m$  matrix associated with an image in grey scale. The "horizontal energy"  $H$  and "vertical energy"  $V$  vectors are defined as follows:

$$H = \sum_{i=1}^p \rho_{li} \quad (1)$$

$$V = \sum_{j=1}^m \gamma_{lj} \quad (2)$$

where  $\rho_{li}$  and  $\gamma_{lj}$  are the  $i$ -th row and the  $j$ -th column of  $I$  respectively.

Let  $A$  be a  $p \times m$  matrix associated with the acquired image and  $R$  a  $q \times n$  matrix associated with the reference one, both in grey scale. The horizontal energy vectors associated with  $A$  and  $R$  are:

$$H_A = \sum_{i=1}^p r_{Ai} \quad (3)$$

$$H_R = \sum_{i=1}^q r_{Ri} \quad (4)$$

with dimensions  $1 \times m$  and  $1 \times n$  respectively and  $m > n$ . A set of  $m - n + 1$  vectors  $H_{Ak}$  can be defined as follows:

$$H_{Ak} = \{h_i^A \in H_A \mid i \in [k; k + n - 1]\} \quad (5)$$

$$k = 1, \dots, m - n + 1$$

where  $h_i^A$  is the  $i$ -th component of the vector  $H_A$ . The horizontal energy consists of the sum of the grey level values associated with the pixels for each column in the image. Therefore, the grey levels which are in an image along the horizontal direction are resumed in only one vector. The vertical energy has the same meaning, but in the vertical direction because the sum of the grey levels is calculated for each row of the image.

It is now possible to evaluate a vector  $C_H$  of  $m - n + 1$  elements, each of which is the correlation coefficient between  $H_R$  and each vector  $H_{Ak}$ . The  $k$ -th element of  $C_H$  is given by the following equation:

$$ch_k = \frac{\sum_{i=1}^n (h_i^R - \bar{h}_R)(h_i^{Ak} - \bar{h}_{Ak})}{\sqrt{\left(\sum_{i=1}^n (h_i^R - \bar{h}_R)^2\right) \left(\sum_{i=1}^n (h_i^{Ak} - \bar{h}_{Ak})^2\right)}} \quad (6)$$

with  $k = 1, \dots, m - n + 1$ , where  $h_i^R$  is the  $i$ -th element of the horizontal energy vector  $H_R$  associated with the reference image,  $\bar{h}_R$  is the mean of the values in  $H_R$ ,  $h_i^{Ak}$  is the  $i$ -th component of the vector  $H_{Ak}$ ,  $\bar{h}_{Ak}$  is the mean of the values in  $H_{Ak}$ .

In the same way the vertical energy vector associated with  $A$  and  $R$  are:

$$V_A = \sum_{j=1}^m c_{Aj} \quad (7)$$

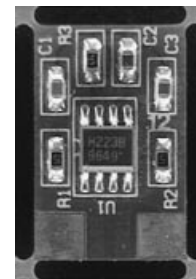


**Figure 3.** First image segmentation: extraction of the board

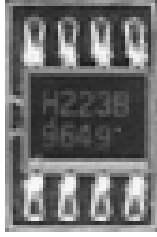


**Figure 4.** Second image segmentation: extraction of the IC

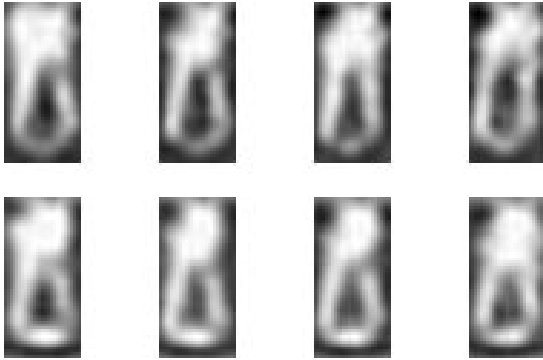


**Figure 5.** Third image segmentation: extraction of the solder joints

$$V_R = \sum_{j=1}^n c_{Rj} \quad (8)$$

whose dimensions are  $1 \times p$  and  $1 \times q$  respectively, with  $p > q$ .

A set of  $p - q + 1$  vectors  $V_{Al}$  can be defined as follows:

$$V_{Al} = \{v_i^A \in V_A \mid i \in [l; l + q - 1]\} \quad (9)$$

$$l = 1, \dots, p - q + 1$$

where  $v_i^A$  is the  $i$ -th component of the vector  $V_A$ . It is now possible to evaluate a vector  $C_V$  of  $p - q + 1$  elements, each of which is the correlation coefficient between  $V_R$  and each vector  $V_{Al}$ .

The  $l$ -th element of  $C_V$  is given by the following equation:

$$c_{hl} = \frac{\sum_{i=1}^q (v_i^R - \bar{v}_R)(v_i^A - \bar{v}_{Al})}{\sqrt{\left( \sum_{i=1}^q (v_i^R - \bar{v}_R)^2 \right) \left( \sum_{i=1}^q (v_i^A - \bar{v}_{Al})^2 \right)}} \quad (10)$$

with  $l = 1, \dots, p - q + 1$ , where  $v_i^R$  is the  $i$ -th element of the vertical energy vector  $V_R$  associated with the reference image,  $\bar{v}_R$  is the mean of the values in  $V_R$ ,  $v_i^A$  is the  $i$ -th component of the vector  $V_{Al}$ ,  $\bar{v}_{Al}$  is the mean of the values in  $V_{Al}$ .

Figures 6 and 7 show the trends of the horizontal and vertical correlation coefficients of an image of the database respectively.

Say  $k_M$  and  $l_M$  are the indexes that denote the positions of the maximum values in  $C_H$  and  $C_V$  respectively. Finally, the ROI is obtained by extracting a  $q \times n$  sub-matrix  $S$  from  $A$ . Matrix  $S$  is defined as follows:

$$S = \{s_{ij}\} \quad (11)$$

where:

$$s_{ij} = a_{i-k_M+1, j-l_M+1} \quad (12)$$

where  $a_{uv}$  is the  $uv$ -th entry of  $A$  and  $i = 1, \dots, q$  and  $j = 1, \dots, n$ .

It is worth noting that  $C_V$  has always one maximum, whereas  $C_H$  has three maxima which correspond to the three boards included in an acquired image. Therefore, the correct value of  $k_M$  is related to the second maximum, which always corresponds to the image under test.

In the second pre-processing step the method previously described is applied once again to the board image obtained from the first step to extract the IC image (figure 4). In this case the reference image is an IC image.

In the last step of the pre-processing stage the images of each solder joint have been extracted from the image of the IC. For this purpose a simple image segmentation algorithm is used because the IC pins are in fixed positions in respect to the IC. The obtained images of the solder joints are shown in figure 5.

#### B. Feature extraction

Two feature types have been extracted from each solder joint image: the geometric features and the wavelet features which are described in detail below.

Let  $\rho(S_{ij})$  denote the mapping of all the pixels of the image of a solder joint. Rosenfeld [14] has defined various geometrical properties of  $\rho(S_{ij})$  that have been employed extensively for pattern recognition. In this work the eight geometrical characteristics used by Howarth and Lotfi (1999) [15], Pal and Mitra (1996) [16], are employed. They are defined as follows:

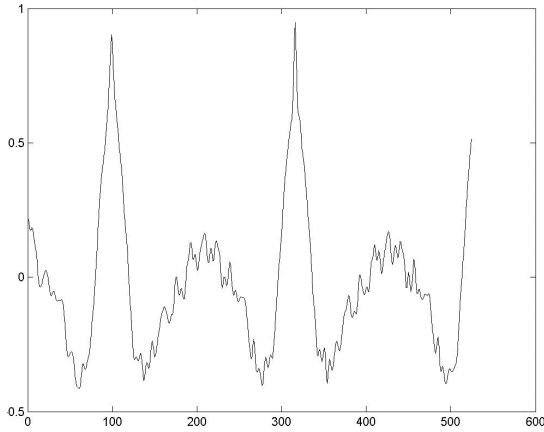


**Figure 6.** Curves of the correlation coefficients between the vectors  $H$

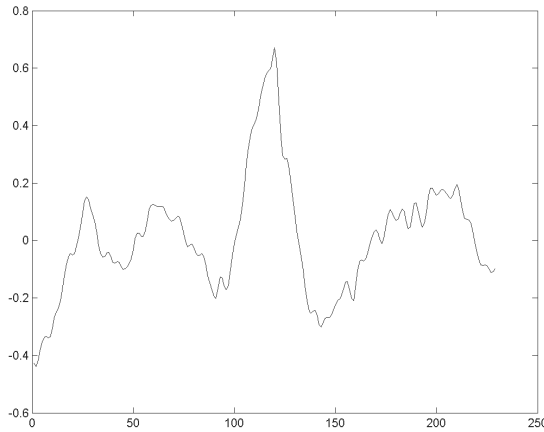


**Figure 7.** Curves of the correlation coefficients between the vectors  $V$

- Area

The area  $A(\rho)$  is defined by:

$$A(\rho) = \sum_{i,j} \rho(S_{ij}) \quad (13)$$

- Perimeter

The perimeter  $P(\rho)$  is defined by:

$$P(\rho) = \sum_j \sum_i \left| \rho(S_{ij}) - \rho(S_{i+1,j}) \right| + \sum_i \sum_j \left| \rho(S_{ij}) - \rho(S_{i,j+1}) \right| \quad (14)$$

- Compactness

The compactness  $C(\rho)$  is defined by:

$$C(\rho) = \frac{A(\rho)}{P^2(\rho)} \quad (15)$$

- Height

The height  $H(\rho)$  is defined by:

$$H(\rho) = \sum_j \left[ \max_i \rho(S_{ij}) \right] \quad (16)$$

- Width

The width  $W(\rho)$  is defined by:

$$W(\rho) = \sum_i \left[ \max_j \rho(S_{ij}) \right] \quad (17)$$

- Length

The length  $L(\rho)$  is defined by:

$$L(\rho) = \max_j \left[ \sum_i \rho(S_{ij}) \right] \quad (18)$$

- Breadth

The breadth  $B(\rho)$  is defined by:

$$B(\rho) = \max_i \left[ \sum_j \rho(S_{ij}) \right] \quad (19)$$

- Index of Area Convergence

The index of area convergence  $I_{ac}(\rho)$  is defined by:

$$I_{ac}(\rho) = \frac{A(\rho)}{L(\rho) \times B(\rho)} \quad (20)$$

This way a vector formed by the eight values of the geometric characteristics has been associated with each solder joint image:

$$V = [A(\rho), P(\rho), C(\rho), H(\rho), W(\rho), L(\rho), B(\rho), I_{ac}(\rho)] \quad (21)$$

The Discrete Wavelet Transform (DWT) has been used in order to extract the wavelet features from each image of the solder joint. How it is employed to obtain the features proposed in this work will be described further on.

The DWT has already been employed for the feature extraction step in the inspection of PCBs [17-19]. Each step to achieve these new features is described below. First consider the definition of the Continuous Wavelet Transform of a signal  $x(t)$ :

$$Wx(s, \tau) = \int_{-\infty}^{+\infty} x(t) \cdot \sqrt{s} \psi(s(t-\tau)) dt \quad (22)$$

The signal  $x(t)$  is decomposed into a family of functions which are the translation and dilation of a unique function  $\psi(t)$ . The function  $\psi(t)$  is called mother wavelet and the corresponding wavelet family is given by:

$$\left[ \sqrt{s}\psi\left(s\left(t-\tau\right)\right) \right]_{(s,\tau)\in\mathbb{R}^2} \quad (23)$$

The parameter  $s$  is called scale parameter while  $\tau$  is the translation parameter.

Let  $\psi_s(t)$  denote the dilation of  $\psi(t)$  with a factor  $s$ :

$$\psi_s(t) = \sqrt{s}\psi(st) \quad (24)$$

and

$$\bar{\psi}_s(t) = \psi_s(-t) \quad (25)$$

The wavelet transform of  $x(t)$  can be rewritten as a convolution product of  $x(t)$  with  $\bar{\psi}_s(t)$ :

$$Wx(s,\tau) = x * \bar{\psi}_s(\tau) \quad (26)$$

In this way a wavelet transform can be viewed as a filtering of  $x(t)$  by a band-pass filter whose impulse response is  $\bar{\psi}_s(t)$ . For high values of the scale  $s$  the result of the filtering is a set of coefficients called approximation coefficients. In this case the wavelet transform of  $x(t)$  can be viewed as a low-pass filtering of  $x(t)$ . On the contrary low values of the scale  $s$  produce a high-pass filtering of  $x(t)$ : the resulting coefficients are called detail coefficients.

The wavelet transform can be discretized by sampling either the scale parameter  $s$  or the translation parameter  $\tau$ . For this purpose it is necessary to fix a sequence of scales  $(\alpha^j)_{j\in\mathbb{Z}}$ , in which  $\alpha$  is the elementary dilation; then the translation parameter  $\tau$  can be sampled at a rate proportional to  $\alpha^j$ . Therefore, the Discrete Wavelet Transform (DWT) is defined by:

$$W_D x(j,k) = Wx\left(\alpha^j, \frac{k\beta}{\alpha^j}\right) = \int_{-\infty}^{+\infty} x(t)\psi_{\alpha^j}\left(t - \frac{k\beta}{\alpha^j}\right) dt \quad (27)$$

The DWT has been implemented by Mallat [20,21]. In Mallat's decomposition algorithm a dyadic scale is employed:

$$\alpha = 2 \quad \beta = 1 \quad (28)$$

This algorithm is an efficient way to implement the DWT of signal  $x(t)$  using filters. It is a classical scheme known in

the signal processing community as a *two-channel subband coder*. It computes a Fast Wavelet Transform (FWT). The first level decomposition of Mallat's algorithm can be schematized as shown in figure 8. The decomposition process can be iterated with successive approximations which are decomposed in turn, so that one signal is broken down into many lower resolution components. This is called the *wavelet decomposition tree*.

For a two dimensional decomposition problem the two-dimensional DWT can be exploited. It works on images as the one-dimensional DWT works on signals. In fact, the algorithm used to extract the wavelet coefficients from the matrix associated with the image of each solder joint has a structure similar to the structure of the one-dimensional algorithm. It performs a one-dimensional DWT of rows and columns according to the chart illustrated in figure 9 which shows the  $j$ -th decomposition step.

At level  $j$  the two-dimensional DWT leads to a decomposition of the approximation coefficients in four components: the approximation coefficients at level  $j+1$  and the details in three directions (horizontal, vertical and diagonal coefficients). In this work, the decomposition has been obtained by means of the haar filter in the low-pass as well as in the high-pass branch of the decomposition scheme. The filter coefficients are defined by the following vectors:

- $L = [0, 7071; 0, 7071]$  low-pass filter
- $H = [-0, 7071; 0, 7071]$  high-pass filter

In each filtering block of the decomposition scheme (figure 9) a convolution product of a single row or column with one of the previous vectors is obtained. In each downsampling block even-indexed columns and rows are selected.

The decomposition process has been stopped at the first level. The matrix associated with each image of the solder joint has dimensions of  $26 \times 16$ , so the wavelet coefficients extracted from the unique decomposition step are four  $13 \times 8$  matrices, but it arises from the experimental results that the

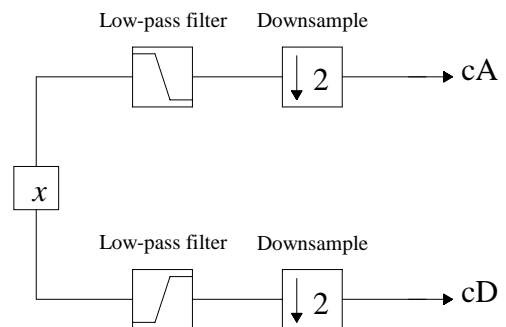
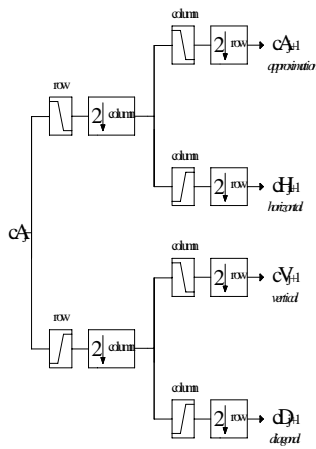


Figure 8. First step of Mallat's algorithm



**Figure 9.**  $j$ -th decomposition step of the two-dimensional DWT

horizontal and diagonal wavelet coefficients do not provide further information than the approximation and vertical ones. For this reason, only the approximation and vertical coefficients have been considered.

The solder joints have been divided in five different types in respect to the amount of solder paste: poor, acceptable poor, good, acceptable excess and excess solder joint.

Five images of the solder types have been assumed as references. For each of these images the approximation and vertical wavelet coefficients have been evaluated. Then the correlation coefficients among these approximation coefficients and those of the image under test are evaluated. In the same way the correlation coefficients among the vertical wavelet coefficients are calculated. Therefore, the vector constituted by these ten values represents the wavelet feature for each solder joint under investigation. Figure 10 shows the construction of the above-mentioned vector. Finally, the vector of the geometric features and the vector of the wavelet features have been normalized. In the following sections the geometric features will be referred as  $G$  features, the wavelet features as  $W$  features. The vector constituted by the joining of the  $G$  and  $W$  features will be called  $GW$  features.

In order to understand better the meanings of the features used in this work their definitions and some explanations are given as follows. The  $G$ -features can be described according to the following verbal definitions: the area is the weighted sum of the regions on which  $\rho$  has constant value weighted by these values; the perimeter is the sum of the absolute difference values of two adjacent pixels along the rows and the columns of the image; the compactness is the fraction of the maximum area that can be encircled by the perimeter

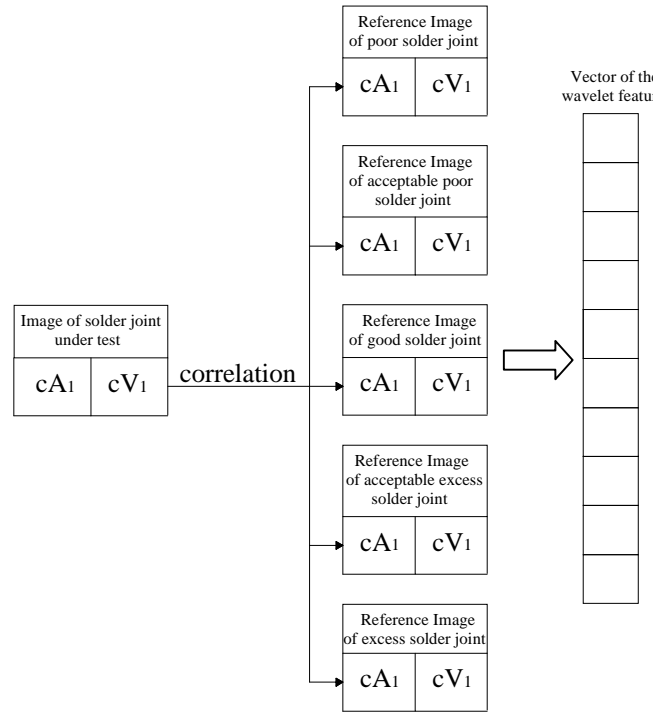


**Figure 10.** Construction of the wavelet feature vector

actually occupied by the region represented by  $\rho$ ; the height is the sum of the maximum values of each row; the width is the sum of the maximum values of each column; the length is the longest expansion of the image in a column; the breadth is the longest expansion of the image in a row; the index of area convergence represents the fraction, which may be improper also, of the maximum area, that can be covered by the length and breadth of the image, actually occupied by the image [16]. Therefore, the  $G$ -features provide some global characteristics of the image under test. These characteristics are shared by all the analyzed images, so those features are able to give a quantitative discrimination of them. The two-dimensional DWT produces a new representation of an image by means of the approximation coefficients and allows the analysis of the characteristics of the image under test along horizontal, vertical and diagonal directions by means of horizontal, vertical and diagonal coefficients. Therefore, the  $W$ -features proposed in this paper take into account the level of similarity among the image under test and the reference one, and the level of similarity among the characteristics along the vertical direction of the two considered images. For these reasons it is possible to argue that the  $G$ -features and the  $W$ -features are able to give the information sufficient to perform the diagnosis, but also that the information produced by the two features is complementary.

*C. Classification*

The last step of this approach is the classification. The vectors of the features associated with the images feed a

MNNS whose scheme is shown in figure 11. It is constituted by two learning levels: the first level is made by an MLP and an LVQ neural network, while the second level is made by an MLP neural network only.

The MNNSs are studied and employed frequently in order to increase the learning accuracy of a classifier, therefore reducing the generalization error and improving the recognition rate in respect to a single neural network. In a MNNS the generalization capability of each neural network is not the same, therefore, different neural networks generate different errors. The combination of these networks makes it possible to improve this capability by suitably handling these errors. There are several strategies able to combine the outputs of these networks. In 1998, Kittler developed a theoretical framework based on the Bayesian theory for combining classifiers [22-24]. In this framework, the most commonly used combination rules, such as the sum rule, the product rule, the min rule, the max rule, the median rule [25,26] and majority vote [13, 25], can be obtained using the Bayesian theory under different assumptions and with different approximations. Another general approach for combining classifiers is the stacking approach [25, 27], in which there are two levels of learning. In particular, the training set of the second level is constructed by the results of the first level. These methods represent the most important schemes that combine individual classifiers achieving better recognition rates.

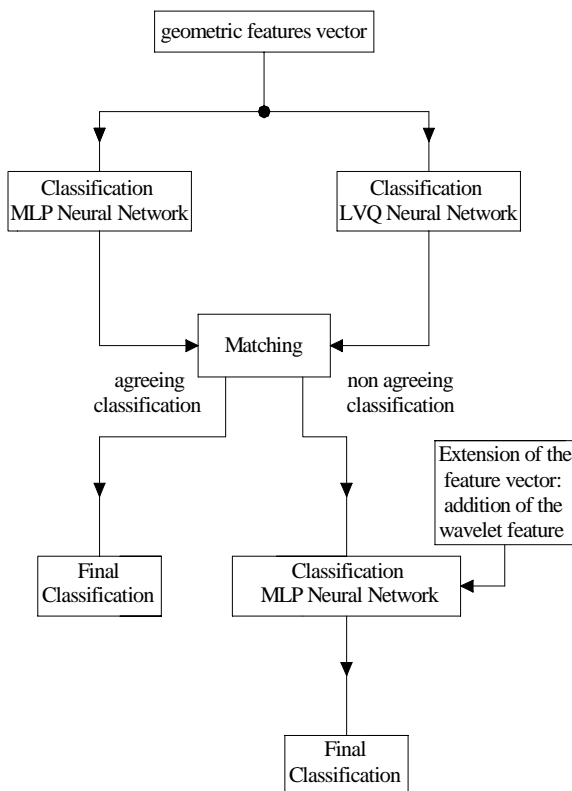


Figure 11. Scheme of the diagnosis system

The MNNS developed in this work could be part of the stacking scheme for combining neural networks, in which the training set of the second level is generated by a simple matching algorithm that compares the outputs of the first level networks. The training set of the second level is generated as the set of those solder joints that give different outputs for the two first level networks. These joints are represented by the  $GW$  features and feed the last MLP level.

In the next section the performance of the proposed MNNS are described in detail, such as the improvement of the recognition rate and diagnosis time in respect to the individual neural networks.

### III. Experimental results

A database of 640 images of solder joints has been analyzed. The solder joint images are divided in the following five different groups: type 1 (insufficient solder), type 2 (acceptable poor solder), type 3 (good solder), type 4 (acceptable excess solder), type 5 (excess solder). Each type of solder joints is represented in figure 12.

The image database has been separated into two sets: a training set constituted by 400 images and a validation set constituted by 240 images of solder joints. The images used for the training and validation sets have been chosen randomly from the original database. The approach described in the previous section has been employed to obtain two geometric feature matrices: the matrix of the training set  $T_G$ , whose dimensions are  $8 \times 400$ ; the matrix of the test set  $V_G$ , whose dimensions are  $8 \times 240$ . In the same



Figure 12. Types of solder joints

way two other wavelet feature matrices have been obtained: the matrix of the training set  $T_w$ , whose dimensions are  $10 \times 400$ ; the matrix of the test set  $V_w$  whose dimensions are  $10 \times 240$ .

Two types of neural networks, MLP and LVQ, have been trained by  $T_G$  and  $T_w$  and tested by  $V_G$  and  $V_w$ . A MLP network with 8 neurons as input layer, 8 neurons as hidden

layer, and 5 neurons as output layer was found to give the best result for the  $G$ -features, while the MLP neural network that performs that best result for the  $W$ -features has 10 neurons as input layer, 10 neurons as hidden layer, and 5 neurons as output layer. Both these networks have a sigmoid activation function in both hidden layers and output layers, while the Levenberg-Marquardt algorithm is used with 100 learning epochs. The LVQ neural networks obtain the best results with the same number of neurons in each layer than the MLP neural networks for  $G$ -features and  $W$ -features respectively. These networks have been trained using a standard learning rate equal to 0.1 and 100 epochs [28].

Since five types of solder joints have been analyzed, an input vector is classified in the  $j$ -th class when the  $j$ -th output value is maximum. Therefore, the class of each input vector  $x$  is defined as follows:

$$c(x) = \{j \text{ iff } y_j = \max_k(y_k) \quad k = 1, \dots, 5\} \quad (29)$$

where  $y_j$  is the  $j$ -th output value with  $j = 1, 2, 3, 4, 5$ .

The neural networks that yield the best results in terms of recognition rate are shown in table 2. In this table the diagnosis time is reported besides the recognition rates; the simulations presented in this section have been run on a Pentium IV under Windows XP. It is worth noting that the recognition rates have close values (the difference between maximum and minimum recognition rate is 2%) but the diagnosis time evaluated employing the geometric features is much lower than the time evaluated employing the wavelet features. The time of classification is 0.12 s for each network while the time for the feature extraction is very different for the two types of features: 0.3 s for geometric features and 7.2 s for wavelet features. For these reasons it is clear that the MLP network fed with geometric features performs the best results, in fact it presents the lower diagnosis time and the best recognition rate.

The diagnosis time is a fundamental parameter in this industrial process, so the various strategies for improving the recognition rate must not neglect the diagnosis time. From this point of view the proposed MNNS improves the recognition rate without losing performance time for the diagnosis.

Below, the experimental results of this system are given in terms of time for the diagnosis and the recognition rate according to the classes defined in 22. The matrix  $T_G$  has been employed to train the two networks of the first learning level: an MLP and an LVQ network.

The results of the first level classification are compared to identify the input vectors that have been classified differently by the two networks.

These vectors and the related solder joints have been wrongly classified at least by one of the networks. The  $GW$  features are then associated with these solder joints to feed the second level of the proposed MNNS: an MLP neural

<b>Geometric Features</b>		
	MLP	LVQ
Training set	$T_G$	$T_G$
Validation set	$V_G$	$V_G$
Recognition rate	95.8%	92.5%
Time for feature extraction (240 pins)	0.3s	0.3s
Time for classification (240 pins)	0.12s	0.12s
Time for diagnosis	7.32s	7.32s
<b>Wavelet Features</b>		
	MLP	LVQ
Training set	$T_W$	$T_W$
Validation set	$V_W$	$V_W$
Recognition rate	94.8%	93.7%
Time for feature extraction (240 pins)	7.2s	7.2s
Time for classification (240 pins)	0.12s	0.12s
Time for diagnosis	7.32s	7.32s

Table 2. Recognition rate and diagnosis times of the single classifiers.

network whose architecture is summarized in table 3. Therefore, a  $18 \times 400$  matrix  $T^E$  of the  $GW$  features which trains this MLP network is defined.

The combination of the first and second classification level outputs constitutes the final classification of the system. The results of the test stage are summarized in table 3. As this table shows, the recognition rate of the overall diagnosis system is 99.5%, while it is lower in the intermediate stage of the classification, when the vectors associated with the images of the solder joints are constituted only by the geometric features: 95.8% for the MLP network and 92.5% for the LVQ one. It is important to highlight that some images of solder joint are not part of the input set  $M$  of the second level of the classifier, even if they have been wrongly classified in the first stage. This occurs when a solder joint is wrongly but not differently classified by the two networks of the first stage. Table 3 shows that the input matrix of the second level is a  $18 \times 25$  matrix  $M$ , even if the number of the solder joints erroneously classified by these two networks is 27. This means that the two networks of the first level have made the same errors in classifying two solder joint images. Therefore, the recognition rate of the overall system is therefore 99.5% even if the second stage MLP classifies all the input vectors without errors. The high recognition rate of the second level MLP (100%) is due to the fact that only a small number of samples have been tested. It is reasonable to assert that a higher number of inputs would produce a lower recognition rate, however the recognition rate of the MNNS is better than that of each network of the first level.

First stage classifier	MLP	LVQ
	G Features	
Recognition rate	95.8%	92.5%
Solder joint wrongly classified	10	17
Solder joint differently classified	25	
Time for diagnosis	0.42s	0.42s
Second stage classifier	MLP	
	GW Features	
Training set	$7^E$	
Validation set	$M (18 \times 25)$	
Neurons of the input layer	18	
Neurons of the hidden layer	12	
Neurons of the output layer	5	
Time for feature extraction	0.74s	
Time for classification	0.13s	
Time for diagnosis	0.87s	
Recognition rate	100%	
Total recognition rate	99.5%	
Total time for diagnosis	1.3s	

Table 3. Recognition rate and diagnosis time of the MNNS

The diagnosis time of the MNNS can be obtained by adding the diagnosis time of the two classification levels: 0.42 s for the first level and 0.87 for the second one. This time is greater than the time spent by the single MLP and LVQ classifiers with geometric features inputs, but it is much lower than the time for the diagnosis of the same networks with the wavelet features inputs. This addition of time is the cost to improve the recognition rate appreciably.

Therefore, it is possible to assert that this architecture is the best compromise in terms of recognition rate and time required for the diagnosis.

#### IV. Conclusion

This paper describes a multiple neural network system for solder joint inspections. The diagnosis is handled as a classification problem with a neural network approach. The proposed MNNS performs the diagnosis; it is constituted by two learning levels, where the second one (an MLP neural network) accomplishes the task of classifying the solder joints that have been classified differently by the first level networks (MLP and LVQ neural networks). Five types of solder joints have been classified in respect to the amount of solder paste. Wavelet coefficients and geometric parameters have been used to extract from a large number of images the features necessary to recognize each solder type. Experimental results have shown that the MNNS assures a good compromise in terms of recognition rate and time required for the diagnosis process in respect to single MLP and LVQ networks with geometric or wavelet features as inputs. Other advantages of this approach are related to the simplicity of the acquisition system; there are no special

illumination systems or advanced X-Y positioning systems required and the features used for diagnosis are evaluated without the knowledge of the industrial physical parameter process.

#### References

- [1] D. Walsh, J. Arena, "Seeing AOI for Six-Sigma PCB Manufacturing", *Electronic Packaging & Production*, 2001.
- [2] P. Krippner, D. Beer, "AOI Testing Positions in Comparison", *Circuit Assembly*, pp. 26-32, 2004.
- [3] T.H. Kim, T.H. Cho, Y.S. Moon, S.H. Park, "Visual inspection system for the classification of solder joints", *Pattern Recognition*, pp. 565-575, 1999.
- [4] K.W. Ko, H.S. Cho, "Solder Joints Inspection Using a Neural Network and Fuzzy Rule-Based Classification Method", *IEEE Transaction on Electronics Packaging Manufacturing*, XXIII (2), pp. 93-103, 2000.
- [5] T.S. Yun, K.J. Sim, H.J. Kim, "Support vector machine-based inspection of solder joints using circular illumination", *Electronics Letters*, XXXVI (11), pp. 949-951, 2000.
- [6] S. Jagannathan, "Automatic Inspection of Wave Soldered Joints Using Neural Networks", *Journal of Manufacturing Systems*, XVI (6), pp. 389-398, 1997.
- [7] A. Fanni, M. Lera, E. Marongiu, A. Montisci, "Automatic Optical Inspection of Electronic Devices using Neural Networks", *Engineering Application of Neural Networks*, Cagliari, Italy, 2001.
- [8] F. Voci, S. Eiho, N. Sugimoto, "Fuzzy Interference Filter And Morphological Operators For Short Circuits Detection In Printed Circuit Board", *International Symposium on Industrial Electronics*, pp. 672-677, 2002.
- [9] C. Neubauer and R. Hanke, "Improving X-Ray Inspection of Printed Circuits Boards by Integration of Neural Network Classifiers", *Electronic Manufacturing Technology Symposium*, pp. 14-18, 1993.
- [10] K.W. Ko, Y.J. Roh, H.S. Cho, H.C. Kim, "A Neural Network Approach to the Inspection of Ball Grid Array Solder Joints on Printed Circuit Boards", *International Joint Conference on Neural Network*, pp. 233-238, 2000.
- [11] R. J. Schalkoff, "Pattern Recognition: Statistical, Structural and Neural Approaches", John Wiley & Sons, 1992.
- [12] R. O. Duda, P. E. Hart, D. G. Stork, "Pattern Classification", J. Wiley & Sons, 2001.
- [13] C. P. Lim, R. F. Harrison, "Online Pattern Classification With Multiple Neural Network Systems: An Experimental Study", *IEEE Transactions on Systems, Man, and Cybernetics*, XXXIII (2), 2003.
- [14] A. Rosenfeld, "Fuzzy Geometry of Image Subsets", *Pattern Recognition Letter*, II, pp. 311-317, 1984.

- [15] M. Howarth, A. Lotfi, "Adaptive Fuzzy Control of Solder Paste Printing: The Identification of Deposit Defects", *Electronics Manufacturing Technology Symposium*, pp. 102-107, 1999.
- [16] S. K. Pal, S. Mitra, "Noisy fingerprint classification using multilayer perceptron with fuzzy geometrical and textural features" *Fuzzy Sets and Systems*, 80, pp. 121-132, 1996.
- [17] T. Taniguchi, D. Kacprzak, S. Yamada, M. Iwahara, "Wavelet-based processing of ECT images for inspection of printed circuit board", *IEEE Transaction on Magnetics*, XXXVII (4), pp. 2790-2793, 2001.
- [18] Z. Ibrahim, S.A.R. Al-Attas, Z. Aspar, M.M. Mokji, "Performance evaluation of wavelet-based PCB defect detection and localization algorithm", *IEEE International Conference on Industrial Technology*, I, pp. 226-231, 2002.
- [19] Z. Ibrahim, S.A.R. Al-Attas, O. Ono, M.M. Mokji, "A noise elimination procedure for wavelet-based printed circuit board inspection system", *Asian Control Conference*, pp. 875-880, 2004.
- [20] S.G. Mallat, "Multifrequency Channel Decompositions of Images and Wavelet Models", *IEEE Transactions on Acoustic, Speech, and Signal Processing*, XXXVII (12), pp. 2091-2110, 1989.
- [21] S.G. Mallat, "A Theory for Multiresolution Signal Decomposition: The Wavelet Representation", *IEEE Transaction on Pattern Analysis and Machine Intelligence*, XI (7), pp. 674-693, 1989.
- [22] J. Kittler, M. Hatef, et al, "On Combining Classifiers", *IEEE Transactions On Pattern Analysis and Machine Intelligence*, XX (3), pp. 226-239, 1998.
- [23] Z. Ahmad, J. Zhang, "Improving Data based Nonlinear Process Modelling through Bayesian Combination of Multiple Neural Networks", *Proceedings of the International Joint Conference on Neural Networks*, IV, pp. 2472 – 2477, 2003.
- [24] L.Y. Yang, Z. Qin, R. Huang, "Design of a Multiple Classifier System", *International Conference on Machine Learning and Cybernetics*, 2004.
- [25] D. Yu, Q. Hu, W. Bao, "Combining Multiple Neural Networks for Classification based on Rough Set Reduction", *IEEE Int. Conf. Neural Networks & Signal Processing*, 2003.
- [26] S. Sohn, C. H. Dagli, "Ensemble of Evolving Neural Networks in Classification", *Neural Processing Letters*, XIX, pp. 191–203, 2004.
- [27] D. Wolpert, "Stacked generalization", *Neural networks*, V, pp.1-57, 1992.
- [28] F.J. Cortijo, N. Perez de la Blanca, "Automatic Estimation of the LVQ-1 Parameters. Application to Multispectral Image Classification", *Proceedings of the 13th International Conference on Pattern Recognition*, pp. 346 – 350, 1996.

## Author Biographies

**Giuseppe Acciani** is Associate Professor of Electric Circuits at Politecnico di Bari, Italy. He received the electrical engineering degree summa cum laude from the University of Bari. After graduation he worked for a Computer Research Centre (CSATA, Italy). In 1985 he joined the Electrical Engineering Department of the Technical University of Bari as Assistant Professor, where he still works as Associate Professor. Currently he teaches "Electric Circuits" and "Intelligent systems for industrial diagnostics". At present his main research interests concern neural networks, in particular unsupervised networks for clustering, and soft computing for non destructive diagnostics.

**Gioacchino Brunetti** received the MSc degree in Electrical Engineering from Politecnico di Bari, Italy, in 2003. Since April 2006 he is a candidate for PhD degree in Electrical Engineering at Politecnico di Bari. His main research interests regard applying neural networks for data classification particularly in the field of the industrial non-destructive diagnostics applications.

**Girolamo Fornarelli** received his Master's degree in Electronic Engineer and the Ph. D. degree in Electrical Engineer from the Politecnico di Bari, where he is Assistant Professor since January 2004. His most research interests include practical and theoretical aspects of neural networks development and soft computing methods in clustering and comparison of multi-dimensional data sets and in non-destructive evaluations. Moreover his research includes analysis of non-linear circuits particularly in developing of the methods to improve the computation time in the simulation of switching circuits.